Characterization of Copper-Zinc-Tin Sulfide Thin Films Produced by Melt-Quenching and PVD

Nabeel Ali Bakr[1], Ali Talib Abbood[1], Falah Ibrahim Mustafa[2] and Kiran Dasharath Diwate[3]
[1]*Department of Physics, College of Science, University of Diyala, 32001 Baqubah, Diyala, Iraq*
[2]*Scientific Research Commission, Ministry of Higher Education and Scientific Research, 10070 Baghdad, Iraq*
[3]*Department of Physics, School of Basic and Applied Sciences, 412207 Pune, India*
nabeelalibakr@yahoo.com, talibali98.at@gmail.com, falah_im@yahoo.com, kdd@jspmuni.ac.in

Keywords: CZTS Thin Films, Melt-quenching, Thermal Evaporation, Structural and Optical Properties, Hall Measurements.

Abstract: Copper–zinc–tin sulfide thin films were prepared through a 2-step route. In the first step, Cu_2ZnSnS_4 powder was produced by the melt-quenching method. These powders were then employed as source materials for thin-film fabrication via thermal evaporation, followed by annealing at 300 °C, 150 °C, and 50 °C. The resulting films were characterized using AFM, FE-SEM, XRD, and FTIR. XRD results confirmed the formation of polycrystalline CZTS films with a tetragonal crystal structure after thermal treatment. The crystallite size increased from approximately 9.53 nm to 16.22 nm as the temperature of annealing increased from 50 °C to 300 °C. Optical studies using Tauc's relation indicated direct band gaps of 1.87, 1.90, and 1.95 eV at 300 °C, 150 °C, and 50 °C, respectively. These values are close to the optimal range for efficient photovoltaic conversion. AFM images showed that post-annealing surfaces were smooth, dense, and uniform, while FTIR spectra identified characteristic functional groups of the material. Hall effect analysis confirmed p-type conductivity for all samples. The annealed CZTS films demonstrate promising properties for use as cost-effective absorber layers in photovoltaic cells.

1 INTRODUCTION

A photovoltaic cell is a device which converts light into electrical energy. Covering only about 1% of the global land surface with photovoltaic cells (with modest assumptions on efficiency and land-use) would suffice to meet the global energy demand [1].

However, the widespread utilization of solar cells is still limited primarily by their high production and installation costs [2]. Conventional solar cells are mainly fabricated from high-purity crystalline silicon, which provides excellent performance but involves expensive purification and processing steps that significantly increase manufacturing costs.

As an alternative, thin-film solar cells have attracted growing interest due to their lower cost and simpler fabrication processes. Thin-film absorber materials typically exhibit absorption coefficients that are about 100 times higher than those of crystalline silicon, meaning that an extremely thin layer can absorb a comparable amount of sunlight.

Additionally, thin-film materials require less stringent purity and crystal quality since grain boundaries in these films can promote charge separation and transport with minimal recombination losses [3].

Consequently, thin-film solar cells offer a cost-effective route for large-scale solar energy production. Among various thin-film absorbers, quaternary chalcogenides such as CZTS have attracted significant attention owing to their favorable optical characteristics, earth-abundant elemental composition, and friendly environmental nature [4]-[6].

CZTS compounds possess a direct allowed bandgap of ~1.4 eV exhibiting p-type conductivity. Despite being relatively new materials, several studies have demonstrated different synthesis approaches for CZTS, encompassing both vacuum-based and non-vacuum techniques.

Solar cells utilizing CZTS absorber layers fabricated by thermal evaporation have achieved a maximum PCE of about 8.4% [7], [8]. Although significant advances have been made, the efficiency of CZTS-based solar cells still remains well below the theoretical limit of approximately 30% [9].

The objective of the present study is to synthesize and characterize nanostructured CZTS thin films prepared via physical evaporation techniques, and to study the influence of fabrication parameters on their structurer as well as their optical, and electrical properties.

2 EXPERIMENTAL PROCEDURES

The Cu_2ZnSnS_4 alloy was synthesized using the melt-quenching method. High-purity elemental powders of copper, zinc, tin, and sulfur were accurately weighed on an electronic balance in stoichiometric proportions corresponding to the desired compound composition.

The weighed powders were thoroughly mixed and transferred into a quartz capsule with a diameter of 30 mm and a length of 100 mm. Prior to sealing, the quartz capsule was evacuated to a pressure of 10^{-5} mbar using a high-vacuum setup.

Once evacuated, the quartz tube was sealed using an LPG–oxygen flame. The sealed capsule was then placed in a muffle furnace [10], where the temperature was increased until it reaches 1100 °C at a rate of 4 °C/min. and kept 15 hours to ensure complete melting and homogenization of the elements.

Immediately after heating, the ampoule was rapidly quenched in ice water to form the desired Cu_2ZnSnS_4 alloy, which was subsequently ground into a fine powder. Thin films were fabricated using the thermal evaporation technique [11]. The prepared alloy powder was placed in a molybdenum boat inside a vacuum chamber evacuated to 10^{-6} mbar.

The alloy was evaporated by gradually raising the current from 100 A to 260 A and keeping it for 12 min. Substrates (Soda-lime) were fixed 18 cm from the source, and multiple cycles were performed to ensure film uniformity. Finally, Annealing was carried out for 2 hours at 300 °C, 150 °C, and 50 °C.

3 RESULTS AND DISCUSION

3.1 XRD of CZTS Absorber Layers

The XRD patterns of Cu_2ZnSnS_4 thin films annealed at 50 °C, 150 °C, and 300 °C are presented in Figure 1. The major diffraction peaks observed at 2θ values of 28.5712°, 32.9541°, 47.4226°, 55.961°, 59.0399°, 69.348°, and 76.3046° correspond to the (112), (020), (220), (132), (224), (040), and (332) crystal planes, respectively, characteristic of the kesterite CZTS phase.

The most intense reflection at 2θ = 28.5712° confirms the (112) preferred orientation, indicating that the films are polycrystalline in nature. This result is consistent with the standard JCPDS card (No. 26-0575) for Cu_2ZnSnS_4 [12] - [17]. As summarized in Table 1, a noticeable shift in the (112) diffraction peak position was observed with increasing annealing temperature.

As the temperature is raised from 50 °C to 150 °C, the 2θ value shifted slightly to higher angles, while a further rise to 300 °C caused the peak to shift toward lower angles. This variation suggests a minor change in lattice parameters, likely associated with strain relaxation and improved crystallinity upon thermal treatment.

Table 1: XRD analysis of Cu_2ZnSnS_4 at different annealing temperatures.

	50 °C	150 °C	300 °C
hkl	(112)	(112)	(112)
2θ	28.642	28.663	28.571

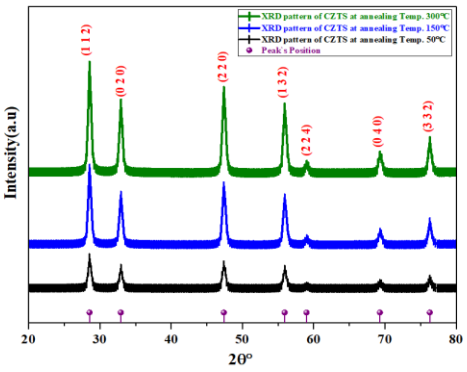

Figure 1: CZTS thin films XRD patterns at various annealing temperatures.

The crystallite size (D) of the prepared thin films was determined using Scherrer's equation:

$$D = \frac{K\,\lambda}{\beta\,Cos\theta}. \quad (1)$$

In this relation, θ represents the diffraction angle, β is FWHM of the corresponding diffraction peak expressed in radians, λ denotes the incident X-ray beam wavelength (0.15406 nm), and K is the Scherrer's constant, which is typically taken as approximately 0.9.

The crystallite size values were calculated from the FWHM of the most intense diffraction peak for each sample, and the obtained results are summarized in Table 2.

Table 2: X-RAY diffraction results of prepared thin films.

2θ (Deg.)	β (rad.)	(hkl)	D (nm)
28.5712	0.52413	112	9.5
32.9541	0.53416	020	11.7
47.4226	0.56260	220	10.08
55.961	0.58610	132	16.2
59.0399	0.53367	224	15.5
69.348	0.58653	040	5.3
76.3046	0.56215	332	9.03

3.2 FTIR Analysis

FTIR spectroscopy was employed to investigate the surface functionalities and identify the characteristic functional groups, impurities, and residual compounds present in the synthesized materials through their IR bands of absorption.

Using FTIR spectroscopy, the CZTS alloy was analyzed to identify the vibrational stretching modes associated with its chemical bonds. The transmission spectrum shown in Figure 2 was recorded within the wavenumber range of interest of 4000–500 cm^{-1}, displays a 3257.1 cm^{-1} peak, corresponding to water and thiourea residues.

The bands near 500 cm^{-1} correspond to the resonance interactions of sulfide ion vibrations within the crystal lattice, while the peaks at 1361.7 and 1635.64 cm^{-1} indicate the formation of a metal–thiourea complex [18], [19].

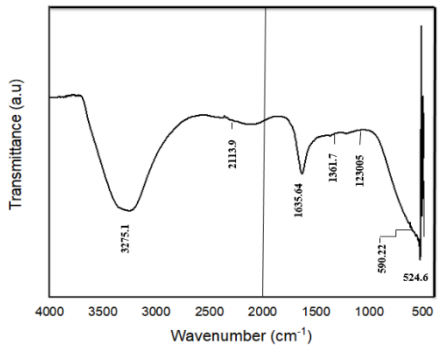

Figure 2: FTIR transmission spectrum of CZTS alloy.

3.3 AFM Images Analysis

The AFM images of CZTS films annealed at various temperatures are presented in Figure 3. The images show a generally uniform surface topography and thickness.

However, slight particle agglomeration is observed in the sample annealed at 50 °C (see Fig. 3a). The samples annealed at higher temperatures exhibit clustered surface features (see Fig. 3b and 3c) with an RMS roughness of approximately 6.78 nm, consistent with the findings of Han *et al.* [20].

The film annealed at 300 °C shown in Figure 3c displays larger, non-uniform clusters and a noticeable increase in surface roughness. The corresponding average and RMS roughness values of the CZTS films are summarized in Table 3.

Overall, the AFM analysis confirms the increase in particle size and surface roughness with higher annealing temperatures which indicates improved grain coalescence and surface reconstruction induced by thermal processing.

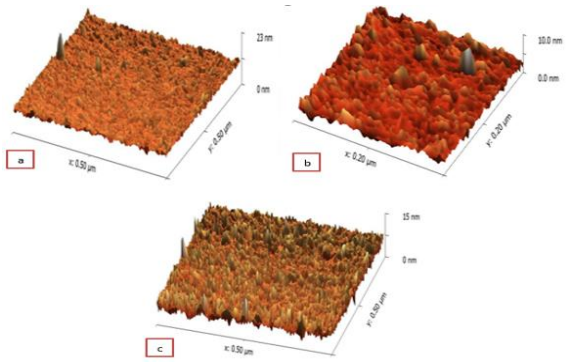

Figure 3: CZTS thin films AFM micrographs of at 50 °C, 150 °C and 300 °C (a, b and c).

Table 3: Surface roughness parameters (average and RMS) and grain size of deposited samples.

Annealing temperature (°C)	Surface roughness average (nm)	RMS roughness (nm)	Average grain size (nm)
50	3.89	4.72	20.63
150	6.783	5.717	57.32
300	10.73	8.218	59.54

3.4 FE-SEM Images Analysis

The FE-SEM micrographs of the films fabricated using physical vapor deposition are shown in Figure 4. The film processed at 50 °C (see Fig. 4a) exhibits a high surface roughness morphology containing numerous pinholes with varying sizes.

At 150 °C (see Fig. 4b), the surface becomes more homogeneous, consisting of small grains aggregated into larger clusters with some remaining voids.

Further increase in the temperature to 300 °C (see Fig. 4c) results in the formation of a smoother and denser surface with significantly enlarged grains.

The micrographs confirm the presence of agglomerated grains with different shapes and sizes, reaching up to approximately 4 µm in diameter.

The growth of larger grains enhances the performance potential of polycrystalline CZTS thin-film solar cells by decreasing the density of grain boundaries, thereby minimizing carrier recombination and extending the diffusion length of minority carriers, which contributes to a higher short-circuit photocurrent [21]-[23]. The corresponding film thicknesses determined for CZTS samples annealed at 300 °C, 150 °C, and 50 °C were approximately 851.6 nm, 700.4 nm, and 550.8 nm, respectively (see Fig. 5a, 5b and 5c).

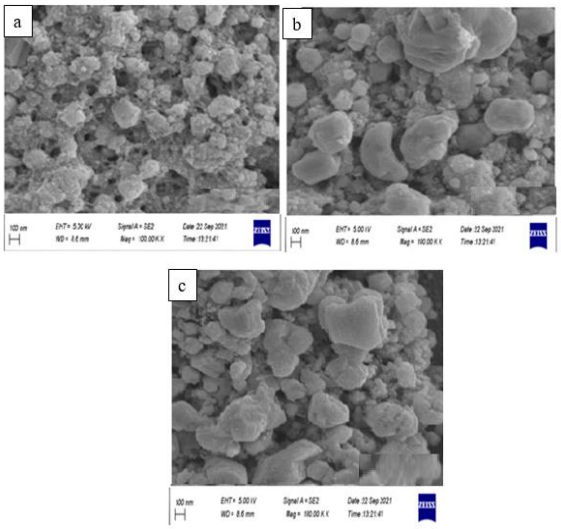

Figure 4: CZTS thin films FE-SEM images, at 50 °C, 150 °C and 300 °C (a, b and c).

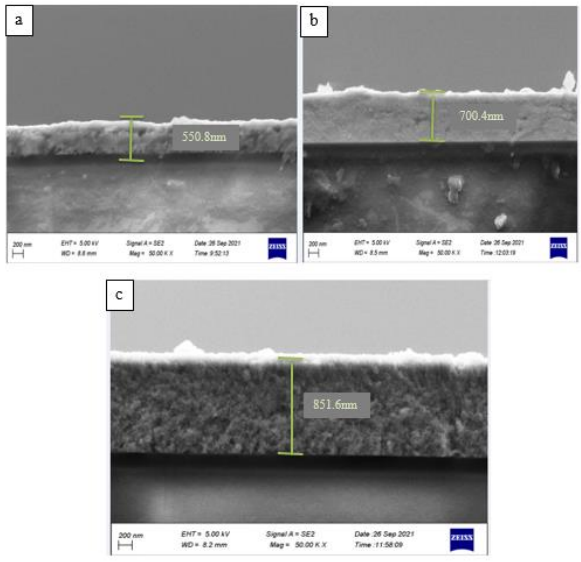

Figure 5: CZTS thin films FE-SEM cross section images at 50 °C, 150 °C and 300 °C (a, b and c).

3.5 EDS Elemental Composition

The EDS analysis of the powders are presented in Figure 6 confirming the presence of all the constituent elements of the compound. The corresponding elemental weight and atomic percentages are summarized in Table 4.

Quantitative EDS analysis verifies that the obtained compositions are close to the ideal stoichiometry of Cu_2ZnSnS_4, indicating successful incorporation of Cu, Zn, Sn, and S elements in the thin films.

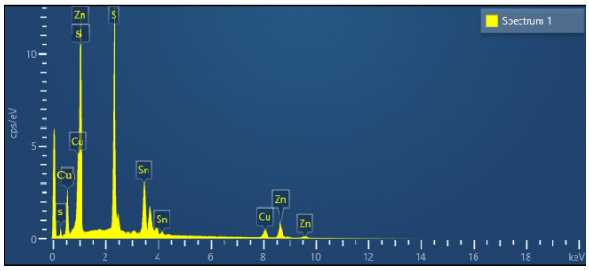

Figure 6: EDS spectrum of CZTS sample.

Table 4: Elemental composition percentages of CZTS sample.

Annealing temperature (°C)	Surface roughness average (nm)	RMS roughness (nm)	Average grain size (nm)
50	3.89	4.72	20.63
150	6.783	5.717	57.32
300	10.73	8.218	59.54

3.6 UV-Vis Spectroscopy

The optical bandgap (Eg) of the deposited films was determined using UV–Vis spectra of absorption represented by Tauc's relation:

$$(\alpha h\vartheta) = C(h\vartheta - E_g)^n, \quad (2)$$

where n is related to the type of electronic transition taken to be ½ for allowed direct transition, α is the absorption coefficient, and B is proportionality constant.

The values of band-gap could be extracted by extrapolation of the straight-line part of $(\alpha h\vartheta)^2$ vs. $(h\vartheta)$ plot to the x-axis (see Fig. 7). The estimated band-gap values for the annealed CZTS thin films were 1.95 eV, 1.90 eV, and 1.87 eV at annealing temperatures of 50°C, 150°C, and 300°C, respectively as shown in Figure 7.

These results are consistent with previously reported data [24], [25].

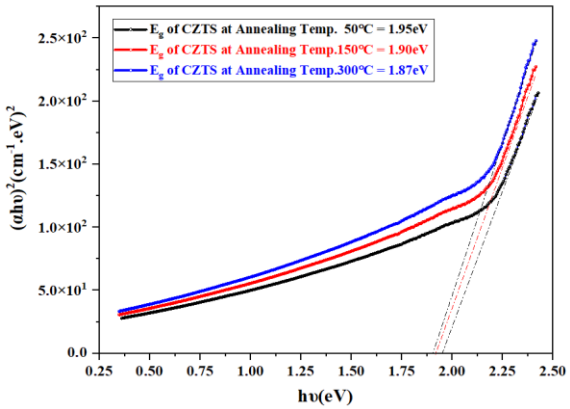

Figure 7: Tauc's plots of CZTS thin films.

A gradual reduction in the band-gap was observed as the annealing temperature increases. This reduction in E_g at higher temperatures, reaching its lowest value at 300 °C, can be attributed to enhanced crystallinity, increased grain size, and reduced structural disorder, which improve the electronic coupling between atoms within the films.

3.7 Electrical Properties

The electrical characteristics of the CZTS thin films, including carrier concentration, mobility, and conductivity, were evaluated at room temperature using a Hall effect measurement system, and the results are summarized in Table 5.

All films exhibited p-type conductivity, confirming that holes are the dominant charge carriers.

The highest carrier concentration of 9.75×10^6 cm^{-3} was obtained at an annealing temperature of 300 °C, indicating improved crystal growth and enhanced film quality. The corresponding electrical conductivity values reached 0.228 $(\Omega \cdot cm)^{-1}$ films processed at 300 °C.

Hall mobility of the films ranged from 87 to 93 $cm^2 \cdot V^{-1} \cdot s^{-1}$, which is consistent with previously reported values [26], [27]. Overall, the electrical conductivity of CZTS thin films increased with higher annealing temperatures, primarily due to the enhancement in carrier concentration and improved crystallinity that facilitate charge transport.

4 CONCLUSIONS

In this work, Cu_2ZnSnS_4 (CZTS) alloy powder was successfully synthesized via the melt-quenching technique and subsequently used as a precursor for the fabrication of CZTS thin films through physical vapor deposition (PVD). Post-deposition annealing at 50 °C, 150 °C, and 300 °C was employed to study the influence of thermal treatment on the structural, morphological, optical, and electrical properties of the produced films.

XRD analysis confirmed the formation of single-phase kesterite CZTS for all samples, with the (112) plane exhibiting the strongest preferred orientation. The observed shift in the (112) peak position and the increase in crystallite size from 9.53 nm to 16.22 nm with higher annealing temperature indicate progressive strain relaxation and enhanced crystallinity. These improvements in film quality were further supported by FTIR measurements, which showed a noticeable reduction in impurity-related absorption bands after annealing, confirming better chemical bonding and reduced residual contaminants.

AFM and FE-SEM analyses demonstrated a clear correlation between annealing temperature, grain coalescence, and surface morphology. Films annealed at 300 °C exhibited larger grain clusters, smoother and denser surfaces, and higher RMS roughness—features that are typically associated with enhanced light absorption, reduced grain-boundary recombination, and improved charge-transport pathways in photovoltaic absorbers. The gradual increase in film thickness with annealing temperature also reflects improved film densification and surface reconstruction.

Table 5: Hall effect properties of CZTS films.

Annealing temperature (°C)	Resistivity (Ω·cm)	Hall coefficient (cm^3/C)	Carrier concentrations $\times10^6$ cm^{-3}	Hall mobility ($cm^2 \cdot V^{-1} \cdot S^{-1}$)
50	22.81	3197.60	1.63	48.00
150	17.54	17.82	3.57	87.80
300	4.38	6.55	9.75	93.28

Optical characterization using Tauc's relation revealed a reduction in the direct band gap from 1.95 eV (50 °C) to 1.87 eV (300 °C). This decrease is attributed to the improved structural order and increased grain size, which facilitate stronger electronic coupling within the lattice. The obtained band-gap range is suitable for heterojunction CZTS solar cells and lies close to the optimal value required for efficient photon absorption in the visible spectrum.

Electrical measurements confirmed p-type conductivity for all samples, with the highest carrier concentration and electrical conductivity observed for films annealed at 300 °C. This enhancement is primarily due to improved crystallinity, reduced defect density, and increased mobility pathways associated with larger grains and better structural ordering.

Overall, the results demonstrate that annealing at 300 °C yields CZTS thin films with the most favorable combination of structural, optical, and electrical properties. These improvements underscore the effectiveness of employing melt-quenched CZTS powders in PVD processes and highlight the potential of the resulting films as promising absorber layers for low-cost, eco-friendly, and scalable thin-film photovoltaic devices.

REFERENCES

[1] A. Saxena et al., "Advanced photovoltaic technology can reduce land requirements and climate impact on energy generation," Communications Earth & Environment, vol. 5, no. 586, 2024, [Online]. Available: https://doi.org/10.1038/s43247-024-01754-4.

[2] C. W. Wadia, A. P. Alivisatos, and D. M. Kammen, "Materials availability expands the opportunity for large-scale photovoltaics deployment," Environmental Science & Technology, vol. 43, no. 6, pp. 2072-2077, 2009, [Online]. Available: https://doi.org/10.1021/es8019534.

[3] J. B. Li, V. Chawla, and B. M. Clemens, "Investigating the role of grain boundaries in CZTS and CZTSSe thin film solar cells with scanning probe microscopy," Advanced Materials, vol. 24, no. 6, pp. 720-723, 2012, [Online]. Available: https://doi.org/10.1002/adma.201103991.

[4] K. I. Nakazawa, "Electrical and optical properties of stannite-type quaternary semiconductor thin films," Japanese Journal of Applied Physics, vol. 27, no. 11R, p. 2094, 1988, [Online]. Available: https://doi.org/10.1143/JJAP.27.2094.

[5] K. Tanaka, N. Moritake, and H. Uchiki, "Preparation of Cu2ZnSnS4 thin films by sulfurizing sol–gel deposited precursors," Solar Energy Materials and Solar Cells, vol. 91, no. 13, pp. 1199-1201, 2007, [Online]. Available: https://doi.org/10.1016/j.solmat.2007.04.001.

[6] M. Grossberg, J. Krustok, K. Timmo, and M. Altosaar, "Radiative recombination in Cu2ZnSnSe4 monograins studied by photoluminescence spectroscopy," Thin Solid Films, vol. 517, no. 7, pp. 2489-2492, 2009, [Online]. Available: https://doi.org/10.1016/j.tsf.2008.11.059.

[7] W. Wang et al., "Device characteristics of CZTSSe thin-film solar cells with 12.6% efficiency," Advanced Energy Materials, vol. 4, no. 7, p. 1301465, 2014, [Online]. Available: https://doi.org/10.1002/aenm.201301465.

[8] B. Shin et al., "Thin-film solar cell with 8.4% power conversion efficiency using an earth-abundant Cu2ZnSnS4 absorber," Progress in Photovoltaics: Research and Applications, vol. 21, no. 1, pp. 72-76, 2013, [Online]. Available: https://doi.org/10.1002/pip.1174.

[9] W. Shockley and H. J. Queisser, "Detailed balance limit of efficiency of p–n junction solar cells," Journal of Applied Physics, vol. 32, no. 3, pp. 510-519, 1961, [Online]. Available: https://doi.org/10.1063/1.1736034.

[10] P. K. Singh, S. K. Sharma, S. K. Tripathi, and D. K. Dwivedi, "Study of dielectric relaxation and thermally activated AC conduction in multicomponent Ge10−xSe60Te30Inx glasses," Results in Physics, vol. 12, pp. 223-236, 2019, [Online]. Available: https://doi.org/10.1016/j.rinp.2018.11.054.

[11] J. Henry, K. Mohanraj, and G. Sivakumar, "XRD, AFM, DRS and photosensitivity of CZTSe thin films prepared by vacuum evaporation," Iranian Journal of Science and Technology, Transactions A: Science, vol. 43, no. 4, pp. 1535-1544, 2019, [Online]. Available: https://doi.org/10.1007/s40995-018-0628-6.

[12] L. Shi, C. Pei, Y. Xu, and Q. Li, "Template-directed synthesis of ordered nanowire arrays of Cu2ZnSnS4 and Cu2ZnSnSe4," Journal of the American Chemical Society, vol. 133, no. 27, pp. 10328-10331, 2011, [Online]. Available: https://doi.org/10.1021/ja203952j.

[13] S. A. Hameed, N. A. Bakr, A. M. Hassan, and A. N. Jasim, "Structural and optical properties of Cu2ZnSnS4 thin films fabricated by chemical spray pyrolysis," in AIP Conference Proceedings, vol. 2213, no. 1, p. 020082, 2020, [Online]. Available: https://doi.org/10.1063/5.0000121.

[14] X. Lin et al., "Synthesis of Cu2ZnxSnySe1+x+2y nanocrystals with wurtzite-derived structure," RSC Advances, vol. 2, no. 26, pp. 9894-9898, 2012, [Online]. Available: https://doi.org/10.1039/C2RA20772K.

[15] E. Jo et al., "8% efficiency Cu2ZnSn(S,Se)4 thin film solar cells on flexible molybdenum foil substrates," ACS Applied Materials & Interfaces, vol. 11, no. 26, pp. 23118-23124, 2019, [Online]. Available: https://doi.org/10.1021/acsami.9b05357.

[16] M. Franckevičius et al., "Efficiency improvement of superstrate CZTSSe solar cells processed by spray pyrolysis," Solar Energy, vol. 185, pp. 283-289, 2019, [Online]. Available: https://doi.org/10.1016/j.solener.2019.04.081.

[17] E. Indubala, K. M. Archana, R. Rajagopalan, and S. Harinipriya, "Selenate precursor for synthesis of CZTSSe: Performance in thin film solar cell," Journal of Alloys and Compounds, vol. 790, pp. 640-649, 2019, [Online]. Available: https://doi.org/10.1016/j.jallcom.2019.03.241.

[18] C. Rein, S. Engberg, and J. W. Andreasen, "Stable, carbon-free inks of Cu2ZnSnS4 nanoparticles synthesized at room temperature," Journal of Alloys and Compounds, vol. 787, pp. 63-71, 2019, [Online]. Available: https://doi.org/10.1016/j.jallcom.2019.02.129.

[19] M. O. Semenenko et al., "RF electromagnetic field treatment of tetragonal kesterite CZTSSe light absorbers," Nanoscale Research Letters, vol. 12, no. 1, p. 1, 2017, [Online]. Available: https://doi.org/10.1186/s11671-017-2146-x.

[20] J. Han, S. W. Shin, M. G. Gang, J. H. Kim, and J. Y. Lee, "Crystallization behavior of co-sputtered Cu2ZnSnS4 precursor," Nanotechnology, vol. 24, no. 9, p. 095706, 2013, [Online]. Available: https://doi.org/10.1088/0957-4484/24/9/095706.

[21] H. Park, Y. Hwang, and B. S. Bae, "Sol–gel processed Cu2ZnSnS4 thin films without sulfurization," Journal of Sol-Gel Science and Technology, vol. 65, no. 1, pp. 23-27, 2013, [Online]. Available: https://doi.org/10.1007/s10971-012-2912-6.

[22] J. Li et al., "Growth of Cu2ZnSnSe4 film under controllable Se vapor composition," ACS Applied Materials & Interfaces, vol. 8, no. 16, pp. 10283-10292, 2016, [Online]. Available: https://doi.org/10.1021/acsami.6b00981.

[23] C. M. Fella et al., "Formation mechanism of Cu2ZnSnSe4 absorber layers during selenization," Journal of Alloys and Compounds, vol. 567, pp. 102-106, 2013, [Online]. Available: https://doi.org/10.1016/j.jallcom.2013.03.004.

[24] N. A. Bakr, Z. T. Khodair, and H. I. Mahdi, "Influence of thiourea concentration on properties of sprayed Cu2ZnSnS4 thin films," International Journal of Materials Science and Applications, vol. 5, no. 6, pp. 261-270, 2016, [Online]. Available: https://doi.org/10.11648/j.ijmsa.20160506.15.

[25] H. Katagiri, "Cu2ZnSnS4 thin film solar cells," Thin Solid Films, vol. 480, pp. 426-432, 2005, [Online]. Available: https://doi.org/10.1016/j.tsf.2004.11.007.

[26] T. Gershon et al., "Photovoltaic device with over 5% efficiency using n-type Ag2ZnSnSe4 absorber," Advanced Energy Materials, vol. 6, no. 22, p. 1601182, 2016, [Online]. Available: https://doi.org/10.1002/aenm.201601182.

[27] T. Gershon et al., "Compositional effects in Ag2ZnSnSe4 thin films and photovoltaic devices," Acta Materialia, vol. 126, pp. 383-388, 2017, [Online]. Available: https://doi.org/10.1016/j.actamat.2016.12.014.